

Multi-Lattice Sampling of Quantum Field Theories via Neural Operator-based Flows

Bálint Máté

François Fleuret

University of Geneva

{balint.mate, francois.fleuret}@unige.ch

Abstract

We consider the problem of sampling discrete field configurations ϕ from the Boltzmann distribution $[d\phi]Z^{-1}e^{-S[\phi]}$, where S is the lattice-discretization of the continuous Euclidean action S of some quantum field theory. Since such densities arise as the approximation of the underlying functional density $[\mathcal{D}\phi(x)]\mathcal{Z}^{-1}e^{-S[\phi(x)]}$, we frame the task as an instance of operator learning. In particular, we propose to approximate a time-dependent operator \mathcal{V}_t whose time integral provides a mapping between the functional distributions of the free theory $[\mathcal{D}\phi(x)]\mathcal{Z}_0^{-1}e^{-S_0[\phi(x)]}$ and of the target theory $[\mathcal{D}\phi(x)]\mathcal{Z}^{-1}e^{-S[\phi(x)]}$. Whenever a particular lattice is chosen, the operator \mathcal{V}_t can be discretized to a finite dimensional, time-dependent vector field V_t which in turn induces a continuous normalizing flow between finite dimensional distributions over the chosen lattice. This flow can then be trained to be a diffeomorphism between the discretized free and target theories $[d\phi]Z_0^{-1}e^{-S_0[\phi]}$, $[d\phi]Z^{-1}e^{-S[\phi]}$. We run experiments on the ϕ^4 -theory to explore to what extent such operator-based flow architectures generalize to lattice sizes they were not trained on and show that pretraining on smaller lattices can lead to speedup over training only a target lattice size.

1 Introduction

Consider S as an action characterizing a quantum field theory, with S representing its discretization to a lattice. Alberg et al. [1] suggest a method for sampling from the lattice quantum field theory described by S . This involves a normalizing flow parameterizing a probability density $q_\theta(\phi)$ of discrete fields over the lattice, and optimizing the parameters θ until $q_\theta(\phi)$ closely approximates $\frac{e^{-S[\phi]}}{Z}$, where $Z = \int [d\phi]e^{-S[\phi]}$ is the normalizing constant.

Operator learning promotes the viewpoint that the lattice/mesh is merely a computational tool, and model should capture the underlying continuous physics. Kovachki et al. [2] term this property of models discretization invariance.¹ In this work, we apply the same idea to the task of sampling from lattice quantum field theories, motivated by the fact that lattice field theories also emerge as the discretization of continuous field theories.

Suppose now that the field theory is defined on some domain D . Once a lattice, as a discretization of D , is chosen, one can construct a continuous normalizing flow [3] as a time-dependent vector field V_t that parametrizes the direction along which probability mass moves. Generalizing this idea, we propose to parametrize a time-dependent operator \mathcal{V}_t from the space of functions on D to itself that defines the direction in which functional probability mass moves. Such an operator can then be used to map the functional distributions $[\mathcal{D}\phi(x)]\mathcal{Z}_0^{-1}e^{-S_0[\phi(x)]}$, $[\mathcal{D}\phi(x)]\mathcal{Z}_1^{-1}e^{-S_1[\phi(x)]}$ to one another. Computationally the operator \mathcal{V}_t can only be accessed by a choice of a lattice which induces a vector field V_t as the discretization of \mathcal{V}_t . We then train this vector field to be a diffeomorphism between the discretized free and target theories, $[d\phi]Z_0^{-1}e^{-S_0[\phi]}$ and $[d\phi]Z_1^{-1}e^{-S_1[\phi]}$. The upside of using an operator-based flow will be that a single model can be used to operate on multiple discretizations of the same underlying continuous system. Figure 1 provides a schematic overview of the objects and their relation in this paragraph.

¹Discretization invariance means that the neural operator evaluated on finer and finer discretizations approximates the continuous operator. Thus, strictly speaking, it is not a requirement of invariance rather that of convergence.

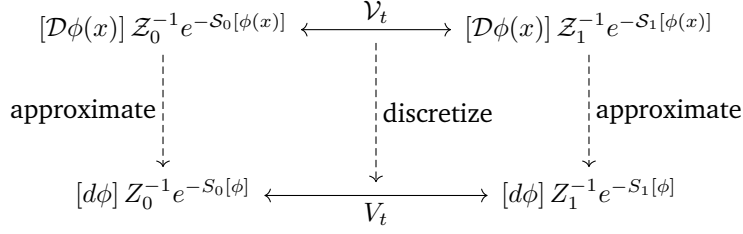


Figure 1: Schematic overview of the probability distributions of interest. The top row shows the functional distributions of the free theory and the target theory connected by the time dependent operator \mathcal{V}_t . Descending to the bottom row means approximating all the objects of the top row on a lattice. In particular, in the bottom row all objects are finite dimensional, well-defined and can be numerically worked with.

The structure of the paper is as follows: Section §2 contains the relevant background on continuous normalizing flows, Boltzmann densities, the ϕ^4 quantum field theory and neural operators. In Section §3 we describe an operator-based normalizing flow architecture that we used in our experiments. Section §4 documents the experiments on the ϕ^4 theory.

2 Background

2.1 Continuous Normalizing Flows

A continuous normalizing flow [3] is a density estimator that operates by pushing forward a simple, usually Gaussian, initial density q_0 along a parametric, time-dependent vector field $V_\theta : [0, 1] \times \mathbb{R}^n \rightarrow \mathbb{R}^n$. Explicitly, the pushforward density q_θ is given by

$$\log q_\theta(x_1) = \log q_0(x_0) + \int_1^0 dt \nabla \cdot V_\theta(t, x_t) \quad (1)$$

where ∇ is the divergence operator in the spatial coordinates and x_t is the integral curve of V_θ that passes through x_1 at $t = 1$. In this work all normalizing flows will be continuous normalizing flows, and we will refer to them as normalizing flows or even just flows for brevity.

Boltzmann distributions The Boltzmann distribution of an energy function² $f : \mathbb{R}^n \rightarrow \mathbb{R}$ is a probability distribution with density function

$$p(x) = \frac{1}{Z} e^{-f(x)} \quad (2)$$

where $Z = \int dx e^{-f(x)}$ is the normalizing constant ensuring that the density function integrates to 1. Boltzmann distributions appear in the context of the canonical ensemble, a statistical ensemble that describes a system in thermal equilibrium with an external heat reservoir. Such Boltzmann distributions describe the molecular systems in thermal equilibrium as well as Wick-rotated quantum field theories. Learning to sample from Boltzmann distributions using only the energy function (i.e. without true samples) can be done by training a normalizing flow[1, 4–16], usually, to minimize the reverse KL divergence

$$KL[q_\theta, p] = \mathbb{E}_{x \sim q_\theta} [\log q_\theta(x) - \log p(x)] \quad (3)$$

$$= \mathbb{E}_{x \sim q_\theta} [\log q_\theta(x) + f(x)] + Z \quad (4)$$

where q_θ is the density realized by the normalizing flow (1). Once a density q_θ , approximating $p = Z^{-1} e^{-f}$, is learnt, one can use importance sampling to correct for small inaccuracies of q_θ when estimating the expected value of an observable \mathcal{O}

$$\langle \mathcal{O} \rangle := \mathbb{E}_{x \sim p} [\mathcal{O}(x)] = \mathbb{E}_{x \sim q_\theta} \left[\mathcal{O}(x) \frac{p(x)}{q_\theta(x)} \right] \quad (5)$$

²Assuming that $\exp(-f)$ is integrable.

2.2 The ϕ^4 (Lattice) Quantum Field Theory³

Let us now consider the Euclidean action on real valued scalar fields $\phi(x)$ with periodic boundary conditions on the D -dimensional hypercube of edge length L , $\phi : (\mathbb{R}/L\mathbb{Z})^D \rightarrow \mathbb{R}$, for some constants m^2 and g

$$S[\phi] = \int_{(\mathbb{R}/L\mathbb{Z})^D} d^D x [(\nabla\phi)^2 + m^2\phi^2 + g\phi^4] \quad (6)$$

where we dropped the argument x of the field $\phi(x)$ for notational convenience. To estimate the expectation value of an observable \mathcal{O} , we need to average over all field configurations that satisfy the boundary conditions, with each configuration weighted by the exponential of the negative action

$$\langle \mathcal{O} \rangle = \frac{\int \mathcal{D}\phi \mathcal{O}[\phi] e^{-S[\phi]}}{\int \mathcal{D}\phi e^{-S[\phi]}} \quad (7)$$

The action S corresponds to the energy function f of a Boltzmann density and the denominator $\mathcal{Z} = \int \mathcal{D}\phi e^{-S[\phi]}$ to the normalizing constant as introduced in Section §2.1.

Equations (6) and (7) describe an infinite dimensional system. To tackle it numerically, one first needs to discretize it to a lattice. This comes at the cost of losing the information contained in the high-frequency components as the highest possible frequency of a periodic function on a lattice with edge length L with N nodes is $\frac{2\pi N}{L}$. The hope is that one can do the same on larger and larger lattices, and as the lattice approaches the continuum limit, the error due to discretization converges to zero.

Discrete representations on lattices

To discretise the action, we consider fields living on the points located at $\left\{ \frac{0}{N}, \frac{L}{N}, \dots, \frac{(N-1)L}{N} \right\}^d$ forming a periodic lattice with cardinality N^D and lattice spacing $a = L/N$. We then turn integrals into sums and differentials into differences between nearest neighbors

$$\partial_i \phi \rightarrow \frac{1}{a} \phi(x + \mu_i) - \phi(x) \quad (8)$$

$$\int_{(\mathbb{R}/L\mathbb{Z})^D} d^D x \rightarrow a^D \sum_x \quad (9)$$

After these substitutions we end up with the following discretised action on the lattice,

$$S[\phi] = a^D \left\{ \frac{1}{a^2} \sum_{x,\mu} (\phi_{x+\mu} - \phi_x)^2 + \sum_x m^2 \phi_x^2 + g \phi_x^4 \right\} \quad (10)$$

where x runs over the lattice sites and μ over the generators of the lattice. It is customary to absorb all the occurrences of a in the above formula by rescaling ϕ

$$\phi \rightarrow a^{D/2-1} \phi, \quad m \rightarrow am, \quad g \rightarrow a^{4-D} g \quad (11)$$

This results in an alternative form of the action

$$S[\phi] = \sum_{x,\mu} (\phi_{x+\mu} - \phi_x)^2 + \sum_x m^2 \phi_x^2 + g \phi_x^4 \quad (12)$$

While the action (12) has the advantage of not being dependent on the lattice spacing a , we will continue working with (10) keeping the relation between different lattice sizes and to the underlying continuous setting explicit.

³We recommend the book [17, Chapter 15] for further details on lattice field theories.

2.3 Neural Operators

Neural operators[2] are trainable function-to-function mappings. In particular, both their domains and codomains are infinite dimensional function spaces. In practice, one works with neural operators by choosing a mesh/lattice $X \subset \mathbb{R}^n$, representing functions by their evaluations on X and let the neural operator operate on this collection of evaluations. By design, neural operators can be evaluated on lattices of different size. Importantly, if a neural operator is applied to a sequence of meshes X_i , approaching the continuum limit $X_i \rightarrow \mathbb{R}^n$, it converges to the underlying continuous operator. The main use case of neural operators is to approximate the solution of partial differential equations, i.e. learn the mapping from an initial condition to the time evolved state after some time Δt (Figure 2), but have also been applied for multi-resolution generative modelling [18, 19]. We will use them for parametrizing a flow, i.e. a vector field \mathcal{V}_t connecting the free theory (base density) to the ϕ^4 -theory (target density) in a way that can be evaluated at any mesh.

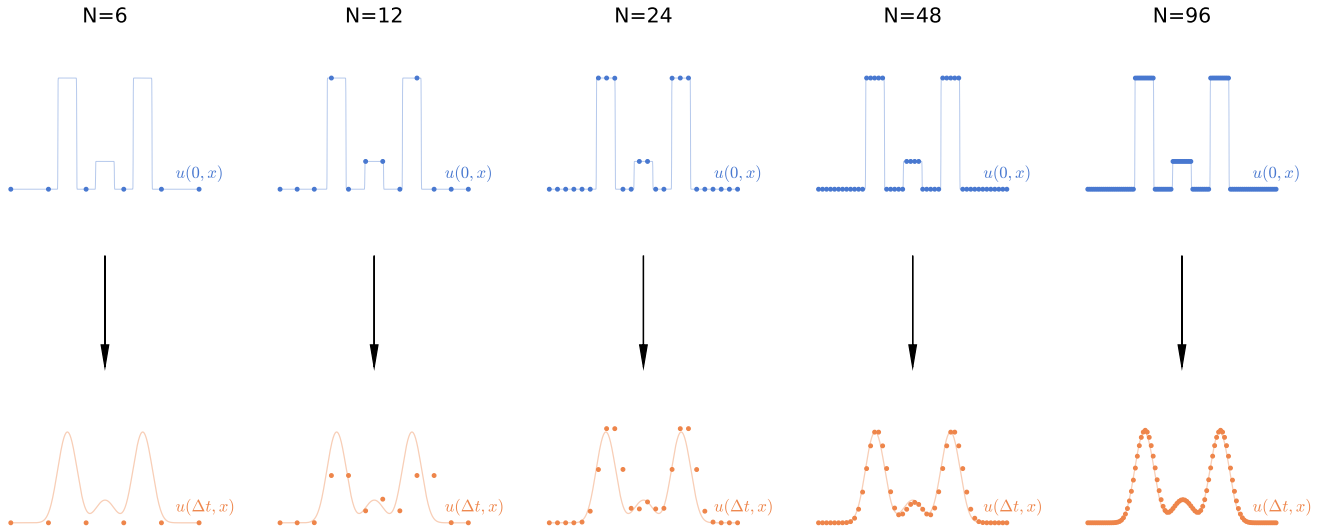


Figure 2: An operator that maps an initial condition $u(0, x)$ (top row) to its time-evolved state $u(\Delta t, x)$ (bottom row). The time evolution is given by the heat equation $\Delta u = \partial_t u$. The blue dots denote the evaluation of $u(0, x)$ on a discrete mesh, while the orange dots denote the output of the operator (a convolution in this case) evaluated on that same mesh. As the mesh gets denser, the operator becomes a better approximation of the map between the continuous $u(0, x)$ (blue curve) and $u(\Delta t, x)$ (orange curve).

3 Flows parametrised by neural operators

When designing the architecture we kept the following considerations in mind

1. The architecture should be a neural operator as described in Section §2.3.
2. The architecture should respect the symmetries of the target density.
3. The architecture should be such that its divergence is reasonably cheap to compute, since it will be integrated over trajectories to compute the density represented by the flow (Equation 1).

The architecture in a nutshell

The output of the model is given by convolving the input with a parametric continuous kernel $K_\theta : (\mathbb{R}/L\mathbb{Z})^D \rightarrow \mathbb{R}$. This guarantees that the first requirement is satisfied, and the second one forces K_θ to be spherically symmetric. Regarding the last one, we take inspiration from Chen and Duvenaud [20], and use the combination of a conditioner function $h_i = c(\phi_{-i})$, whose output at any coordinate is independent of the same coordinate of the input, and a transformer function $f_i = \tau(h_i, \phi_i)$ function that combines the conditioning and the input. The advantage of this architecture is that its divergence is $\sum_i (\partial_2 \tau)$ and thus the capacity of c can be cheaply increased.

The architecture in detail

Let now $\phi \in \mathbb{R}^{N \times \dots \times N}$ be a discretized scalar field on a lattice. The architecture then consists of the following sequence of steps, where the subscript θ denotes trainable parameters,

1. Use a per-node neural network f_θ to embed the field values, $\phi_{emb} = f_\theta(\phi) \in \mathbb{R}^{c \times N \times \dots \times N}$.
2. Use a neural network to parametrize c -many continuous spherically symmetric kernels $K_\theta(r)$. Let then \tilde{K}_θ be the evaluation of the continuous kernels on the lattice.
3. Mask out the origin of the discrete kernel, i.e. set $\tilde{K}_\theta[:, \mathbf{0}] = 0$.
4. Perform a channel-wise convolution $\phi_{emb} \star \tilde{K}_\theta$ and denote the result by $C \in \mathbb{R}^{c \times N \times \dots \times N}$. Because of the previous step, C_i is independent of ϕ_i , and we will call it the conditioner [20].
5. Apply a per-node neural network τ_θ to the concatenation (C, ϕ_{emb}) with output $Y = \tau_\theta(C, \phi_{emb}) \in \mathbb{R}^{T \times N \times \dots \times N}$.
6. Contract the first dimension of Y with a vector of length T that only depends on time.
7. Finally, denoting all the above steps as i , we set the output of the model to be $V(\phi, t) = \frac{1}{2} * (i(\phi, t) - i(-\phi, t))$. This enforces the \mathbb{Z}_2 symmetry of the system.

To compute the divergence of the architecture one needs the Jacobians of the per-point operations f_θ and τ_θ , K_θ does not have to be differentiated through.

The free theory as an initial density

The normalizing flow architecture described in Section §2.1 requires an initial density from which samples can easily be drawn. Instead of sampling from a standard gaussian at every node, we choose a more physical initial density by setting $g = 0$ in the action (10). This results in the free theory with a gaussian Boltzmann density that becomes diagonal in momentum space. Position and momentum space are related by a discrete Fourier transform

$$\phi_x = \frac{1}{\sqrt{N^D}} \sum_p \tilde{\phi}_p e^{i2\pi \langle p, x \rangle} \quad (13)$$

$$\tilde{\phi}_p = \frac{1}{\sqrt{N^D}} \sum_x \phi_x e^{-i2\pi \langle p, x \rangle} \quad (14)$$

where p runs over $\left\{ -\frac{\lfloor N/2 \rfloor}{L}, \dots, \frac{0}{L}, \dots, \frac{\lceil (N-1)/2 \rceil}{L} \right\}^D$ and the prefactor $\frac{1}{\sqrt{N^D}}$ makes the map $\{\phi_x\} \leftrightarrow \{\tilde{\phi}_p\}$ unitary. The covariance matrix of the free theory is diagonalized in the momentum basis $\frac{1}{\sqrt{N^D}} e^{2\pi i \langle x, p \rangle}$ with eigenvalues

$$S \left[\frac{1}{\sqrt{N^D}} e^{2\pi i \langle x, p \rangle} \right] = a^D \left(m^2 + \frac{1}{a^2} \sum_\mu 2 - 2 \cos(2\pi p_\mu a) \right) \quad (15)$$

To constrain the sampling to real valued fields, we sample p from the hermitian symmetric subspace of *real dimension* N^D of the Fourier-space of *complex dimension* N^D .

4 Experiments

4.1 Multi-lattice sampling in $D = 1$ dimension

We now work in $D = 1$ dimensions. Strictly speaking, a one dimensional lattice does not correspond to a quantum field theory, rather it describes the trajectory of a quantum mechanical particle in a potential. Nonetheless, it's the simplest setup in which we can experiment and serves as a good starting point. We also fix $L = 4, m^2 = -4, g = 1$ and train a single model for 5000 steps with mesh size uniformly sampled at each training step from $N = L/a \in \{4, 8, 16, \dots, 128\}$. We then evaluate performance on lattices of size $N = L/a$ up to 512 by sampling from the trained model to calculate the effective sample size (Figure 3)

$$ESS = \frac{\left(\frac{1}{N} \sum_i w_i \right)^2}{\frac{1}{N} \sum_i w_i^2} \quad (16)$$

where w_i is the importance weight $p(\phi_i)/q_\theta(\phi_i)$. We also estimate expectation values of the magnetization and its absolute value (Figure 3)

$$M[\phi] := \frac{1}{N^D} \sum_x \phi(x) \quad |M|[\phi] := \frac{1}{N^D} \left| \sum_x \phi(x) \right| \quad (17)$$

and of the two-point correlation function (Figure 4)

$$G(x, y)[\phi] := \phi(x)\phi(y). \quad (18)$$

We also compare flattened samples from the model against the one-dimensional Boltzmann density of the potential $m^2\phi^2 + g\phi^4$ (Figure 5).

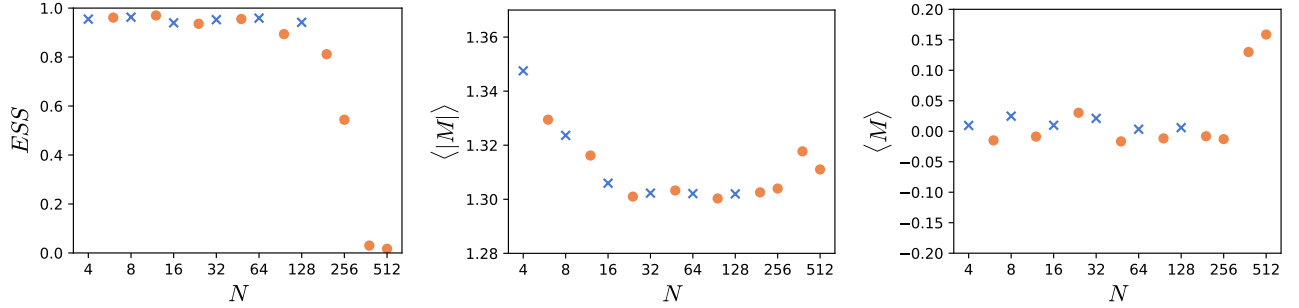


Figure 3: Experiment 4.1. $ESS, \langle M \rangle, \langle |M| \rangle$ computed from 16384 samples at different lattice sizes. The blue crosses correspond to lattice sizes that the model was trained on, while orange dots denote lattice sizes unseen by the network during training.

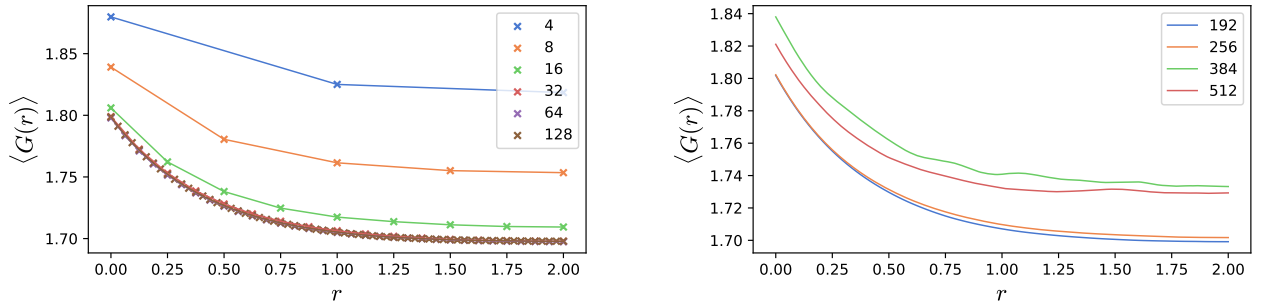


Figure 4: Experiment 4.1. The two-point correlation function $G(x, y)$ computed from 16384 samples on lattices the model was trained on (left) and on lattices the model was not trained on (right). Because of the symmetries of the task the correlation function only depends on the distance $r = |x - y|$, thus the function $G(r)$ is plotted.

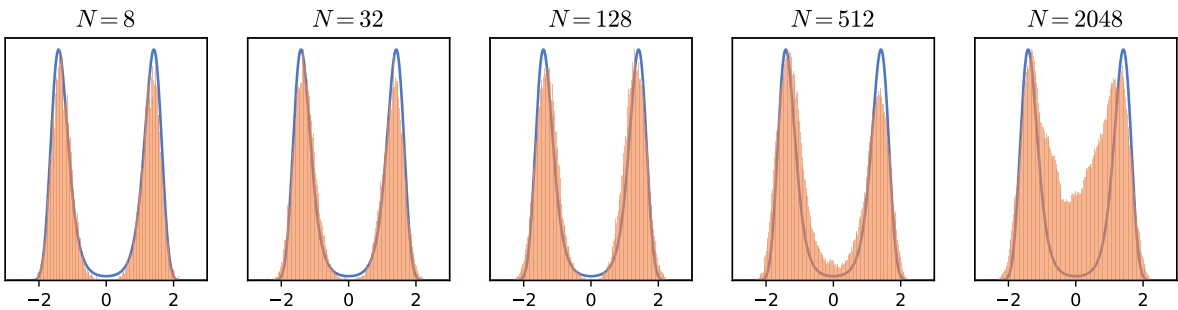


Figure 5: Experiment 4.1. Flattened samples (orange histogram) of the model at different lattice sizes $N = L/a$ compared to the one-dimensional Boltzmann density $e^{-m^2\phi^2 - g\phi^4}$ (blue curve).

4.2 Multi-lattice sampling in $D = 2$ dimensions

In this experiment we work with $D = 2, L = 6, m^2 = -4, g = 6.975$ (the smallest system of [15]). We train for 15000 steps with $N = L/a$ uniformly sampled from $[6, 7, 8, \dots, 32]$ at each training step. We evaluate the trained model on lattices up to size 64×64 . We report the effective sample size, as well as the expected value of the observables M and $|M|$ (Table 1) and the estimated correlation function at different lattice sizes (Figure 6).

Table 1: Experiment 4.2. Effective sample size and expected value of the observables $M, |M|$ computed at different lattice sizes. The four rightmost columns correspond to lattice sizes the model was not trained on.

$N \times N$	8×8	12×12	16×16	20×20	24×24	32×32	40×40	48×48	56×56	64×64
ESS	0.984	0.992	0.985	0.979	0.969	0.917	0.568	0.136	0.038	0.002
$\langle M \rangle$	-0.001	0.001	0.001	0.000	-0.000	-0.000	-0.001	-0.001	-0.001	0.001
$\langle M \rangle$	0.103	0.074	0.062	0.056	0.052	0.047	0.043	0.040	0.041	0.037

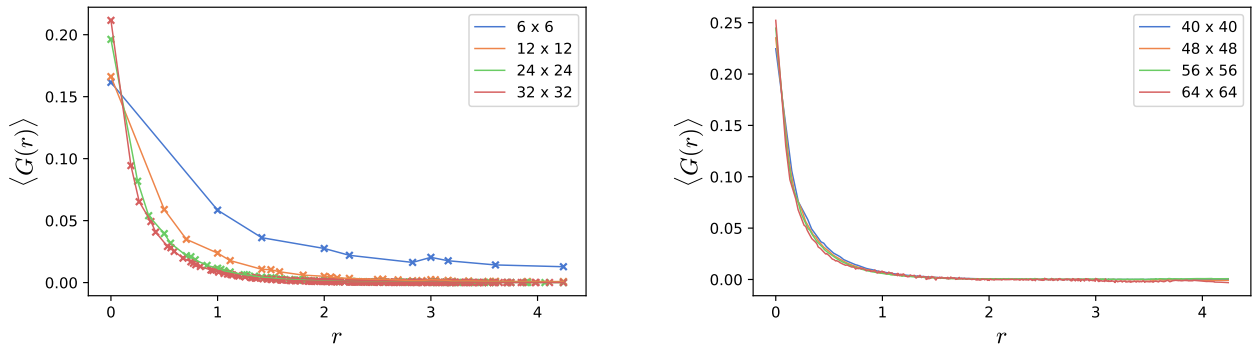


Figure 6: Experiment 4.2. The two-point correlation function $G(x, y)$ of the second experiment computed from 16384 samples on lattices the model was trained on (left) and on lattices the model was not trained on (right). Because of the symmetries of the task the correlation function only depends on the distance $r = |x - y|$, thus the function $G(r)$ is plotted.

As in the previous experiment, the model does not extrapolate well to lattice sizes much higher than those that it was trained on. It is worth noting nonetheless that performance as a function of lattice size does not drop suddenly and it is still acceptable on slightly higher lattice size than the largest training lattice. This observation motivates the following experiment.

4.3 Faster convergence on a target lattice size by pretraining on smaller ones

In this experiment we consider the target $D = 2, L = 12, m^2 = -4, g = 5.276, N = 64$. Instead of training directly on the $N = 64$ lattice, we pretrain on a sequence of smaller lattices as they are significantly cheaper to work on. We start training on a 12×12 lattice for 2000 steps, after which we train on lattices of size $16 \times 16, 20 \times 20, 24 \times 24, 28 \times 28, 32 \times 32, 36 \times 36, 40 \times 40, 44 \times 44, 48 \times 48, 52 \times 52, 56 \times 56, 60 \times 60$ for 250 training steps each. Finally, we train on the target size 64×64 for 1000 steps. As a baseline, we also train the same architecture only on the target size for the same total number of steps (6000). While the performance, as measured by the effective sample size on target lattice, is comparable after training (Table 2), the training procedure that "trained through" the smaller lattices was ~ 2.4 -times quicker to train (Figure 7). Figure 8 shows the estimated correlation function at different lattice sizes computed from model checkpoints saved right after taking the last training step on the given lattice size.

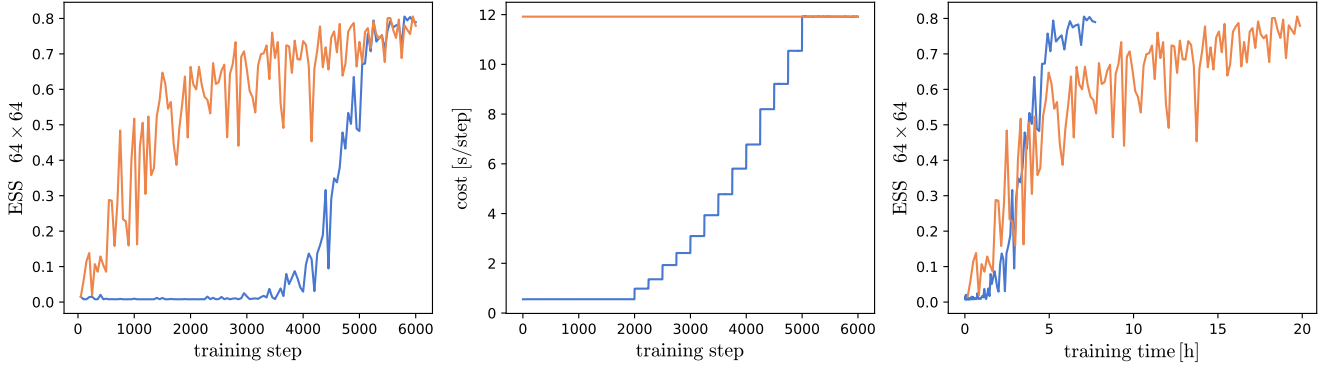


Figure 7: Experiment 4.3. ESS estimated during training on 128 samples plotted against the number of training steps (left) and training time (right). Time required to take a single step (center). All plots contain two curves, one for the model that is trained on the sequence of increasing lattice sizes (blue) and one that is only trained on the 64×64 lattice (orange). We also refer the reader to Figure 9 in the appendix that shows the ESS values on all lattice sizes during training.

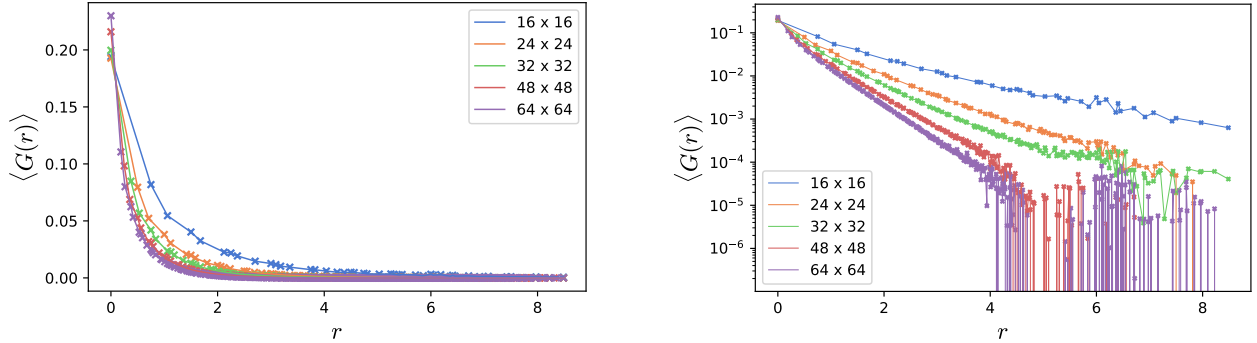


Figure 8: Experiment 4.3. The two-point correlation function $G(x, y)$ computed from 16384 samples with (right) and without (left) log-scaled y -axis. These curves are computed from model checkpoints saved right after taking the last training step on the given lattice size. Because of the symmetries of the task the correlation function only depends on the distance $r = |x - y|$, thus the function $G(r)$ is plotted.

Table 2: Experiment 4.3. ESS values on 16384 samples from the trained model. Since training on larger lattices degrades performance on smaller ones (Figure 9), the model is evaluated directly after the last training step has been performed on a given lattice size. The final column marked with \flat denotes the baseline model.

$N \times N$	16×16	24×24	32×32	48×48	64×64	$64 \times 64^\flat$
ESS	0.8937	0.8628	0.8771	0.7736	0.7824	0.7722

5 Conclusion

In this work we explored the idea of using operator-based normalizing flows for sampling from the ϕ^4 quantum field theory. Experiments 4.1 and 4.2 showed that models trained on a collection of lattices do not generalize zero-shot to lattice sizes much larger than those of the training set. They do generalize with a reasonable performance to lattice sizes slightly larger than the ones it has been trained on. Making use of this observation, in experiment 4.3 we show that training a model on a sequence of meshes of increasing size leads to faster training compared to training directly on the target lattice size.

6 Acknowledgement

The authors were supported by the Swiss National Science Foundation under grant number CRSII5_193716 - “Robust Deep Density Models for High-Energy Particle Physics and Solar Flare Analysis (RODEM)”. We express our appreciation of the Python ecosystem [21] and its libraries that made this work possible. In particular, the experimental part of the paper relies heavily on JAX [22], Flax [23], optax [22], numpy [24], hydra [25], matplotlib [26], jupyter [27] and weights&biases [28]. We thank Samuel Klein for discussions.

References

- [1] Michael S Albergo, Gurtej Kanwar, and Phiala E Shanahan. Flow-based generative models for markov chain monte carlo in lattice field theory. *Physical Review D*, 100(3):034515, 2019.
- [2] Nikola Kovachki, Zongyi Li, Burigede Liu, Kamyar Azizzadenesheli, Kaushik Bhattacharya, Andrew Stuart, and Anima Anandkumar. Neural operator: Learning maps between function spaces. *arXiv preprint arXiv:2108.08481*, 2021.
- [3] Ricky TQ Chen, Yulia Rubanova, Jesse Bettencourt, and David K Duvenaud. Neural ordinary differential equations. *Advances in neural information processing systems*, 31, 2018.
- [4] Michael S. Albergo, Denis Boyda, Daniel C. Hackett, Gurtej Kanwar, Kyle Cranmer, Sébastien Racanière, Danilo Jimenez Rezende, and Phiala E. Shanahan. Introduction to normalizing flows for lattice field theory, 2021. URL <https://arxiv.org/abs/2101.08176>.
- [5] Michael S. Albergo, Denis Boyda, Kyle Cranmer, Daniel C. Hackett, Gurtej Kanwar, Sébastien Racanière, Danilo J. Rezende, Fernando Romero-López, Phiala E. Shanahan, and Julian M. Urban. Flow-based sampling in the lattice schwinger model at criticality, 2022. URL <https://arxiv.org/abs/2202.11712>.
- [6] Ryan Abbott, Michael S. Albergo, Denis Boyda, Kyle Cranmer, Daniel C. Hackett, Gurtej Kanwar, Sébastien Racanière, Danilo J. Rezende, Fernando Romero-López, Phiala E. Shanahan, Betsy Tian, and Julian M. Urban. Gauge-equivariant flow models for sampling in lattice field theories with pseudofermions, 2022. URL <https://arxiv.org/abs/2207.08945>.
- [7] Michael S. Albergo, Gurtej Kanwar, Sébastien Racanière, Danilo J. Rezende, Julian M. Urban, Denis Boyda, Kyle Cranmer, Daniel C. Hackett, and Phiala E. Shanahan. Flow-based sampling for fermionic lattice field theories. *Physical Review D*, 104(11), dec 2021. doi: 10.1103/physrevd.104.114507. URL <https://doi.org/10.1103/PhysRevD.104.114507>.
- [8] Denis Boyda, Gurtej Kanwar, Sébastien Racanière, Danilo Jimenez Rezende, Michael S. Albergo, Kyle Cranmer, Daniel C. Hackett, and Phiala E. Shanahan. Sampling using $SU(n)$ gauge equivariant flows. *Phys. Rev. D*, 103:074504, Apr 2021. doi: 10.1103/PhysRevD.103.074504. URL <https://link.aps.org/doi/10.1103/PhysRevD.103.074504>.
- [9] Frank Noé, Simon Olsson, Jonas Köhler, and Hao Wu. Boltzmann generators – sampling equilibrium states of many-body systems with deep learning, 2018. URL <https://arxiv.org/abs/1812.01729>.
- [10] Jonas Köhler, Leon Klein, and Frank Noé. Equivariant flows: Exact likelihood generative learning for symmetric densities, 2020. URL <https://arxiv.org/abs/2006.02425>.
- [11] Kim A. Nicoli, Shinichi Nakajima, Nils Strodthoff, Wojciech Samek, Klaus-Robert Müller, and Pan Kessel. Asymptotically unbiased estimation of physical observables with neural samplers. *Physical Review E*, 101(2), feb 2020. doi: 10.1103/physreve.101.023304. URL <https://doi.org/10.1103/PhysRevE.101.023304>.
- [12] Kim A Nicoli, Christopher J Anders, Lena Funcke, Tobias Hartung, Karl Jansen, Pan Kessel, Shinichi Nakajima, and Paolo Stornati. Estimation of thermodynamic observables in lattice field theories with deep generative models. *Physical review letters*, 126(3):032001, 2021.
- [13] Kim A Nicoli, Christopher J Anders, Tobias Hartung, Karl Jansen, Pan Kessel, and Shinichi Nakajima. Detecting and mitigating mode-collapse for flow-based sampling of lattice field theories. *arXiv preprint arXiv:2302.14082*, 2023.

- [14] Pim de Haan, Corrado Rainone, Miranda C. N. Cheng, and Roberto Bondesan. Scaling up machine learning for quantum field theory with equivariant continuous flows, 2021. URL <https://arxiv.org/abs/2110.02673>.
- [15] Mathis Gerdes, Pim de Haan, Corrado Rainone, Roberto Bondesan, and Miranda C. N. Cheng. Learning lattice quantum field theories with equivariant continuous flows, 2022.
- [16] Bálint Máté and François Fleuret. Learning interpolations between boltzmann densities. *Transactions on Machine Learning Research*, 2023. ISSN 2835-8856. URL <https://openreview.net/forum?id=TH6YrEcbth>.
- [17] Jos Thijssen. *Computational Physics*. Cambridge University Press, 2 edition, 2007. doi: 10.1017/CBO9781139171397.
- [18] Vikram Voleti, Chris Finlay, Adam Oberman, and Christopher Pal. Multi-resolution continuous normalizing flows. *arXiv preprint arXiv:2106.08462*, 2021.
- [19] Paul Hagemann, Lars Ruthotto, Gabriele Steidl, and Nicole Tianjiao Yang. Multilevel diffusion: Infinite dimensional score-based diffusion models for image generation. *arXiv preprint arXiv:2303.04772*, 2023.
- [20] Ricky TQ Chen and David K Duvenaud. Neural networks with cheap differential operators. *Advances in Neural Information Processing Systems*, 32, 2019.
- [21] Guido Van Rossum and Fred L Drake Jr. *Python reference manual*. Centrum voor Wiskunde en Informatica Amsterdam, 1995.
- [22] Igor Babuschkin, Kate Baumli, Alison Bell, Surya Bhupatiraju, Jake Bruce, Peter Buchlovsky, David Budden, Trevor Cai, Aidan Clark, Ivo Danihelka, Antoine Dedieu, Claudio Fantacci, Jonathan Godwin, Chris Jones, Ross Hemsley, Tom Hennigan, Matteo Hessel, Shaobo Hou, Steven Kapturowski, Thomas Keck, Iurii Kemaev, Michael King, Markus Kunesch, Lena Martens, Hamza Merzic, Vladimir Mikulik, Tamara Norman, George Papamakarios, John Quan, Roman Ring, Francisco Ruiz, Alvaro Sanchez, Rosalia Schneider, Eren Sezener, Stephen Spencer, Srivatsan Srinivasan, Wojciech Stokowiec, Luyu Wang, Guangyao Zhou, and Fabio Viola. The DeepMind JAX Ecosystem, 2020. URL <http://github.com/deepmind>.
- [23] Jonathan Heek, Anselm Levskaya, Avital Oliver, Marvin Ritter, Bertrand Rondepierre, Andreas Steiner, and Marc van Zee. Flax: A neural network library and ecosystem for JAX, 2023. URL <http://github.com/google/flax>.
- [24] Charles R. Harris, K. Jarrod Millman, Stéfan J. van der Walt, Ralf Gommers, Pauli Virtanen, David Cournapeau, Eric Wieser, Julian Taylor, Sebastian Berg, Nathaniel J. Smith, Robert Kern, Matti Picus, Stephan Hoyer, Marten H. van Kerkwijk, Matthew Brett, Allan Haldane, Jaime Fernández del Río, Mark Wiebe, Pearu Peterson, Pierre Gérard-Marchant, Kevin Sheppard, Tyler Reddy, Warren Weckesser, Hameer Abbasi, Christoph Gohlke, and Travis E. Oliphant. Array programming with NumPy. *Nature*, 585(7825):357–362, September 2020. doi: 10.1038/s41586-020-2649-2. URL <https://doi.org/10.1038/s41586-020-2649-2>.
- [25] Omry Yadan. Hydra - a framework for elegantly configuring complex applications. Github, 2019. URL <https://github.com/facebookresearch/hydra>.
- [26] J. D. Hunter. Matplotlib: A 2d graphics environment. *Computing in Science & Engineering*, 9(3):90–95, 2007. doi: 10.1109/MCSE.2007.55.
- [27] Fernando Pérez and Brian E. Granger. IPython: a system for interactive scientific computing. *Computing in Science and Engineering*, 9(3):21–29, May 2007. ISSN 1521-9615. doi: 10.1109/MCSE.2007.53. URL <https://ipython.org>.
- [28] Lukas Biewald. Experiment tracking with weights and biases, 2020. URL <https://www.wandb.com/>. Software available from wandb.com.

Additional figures

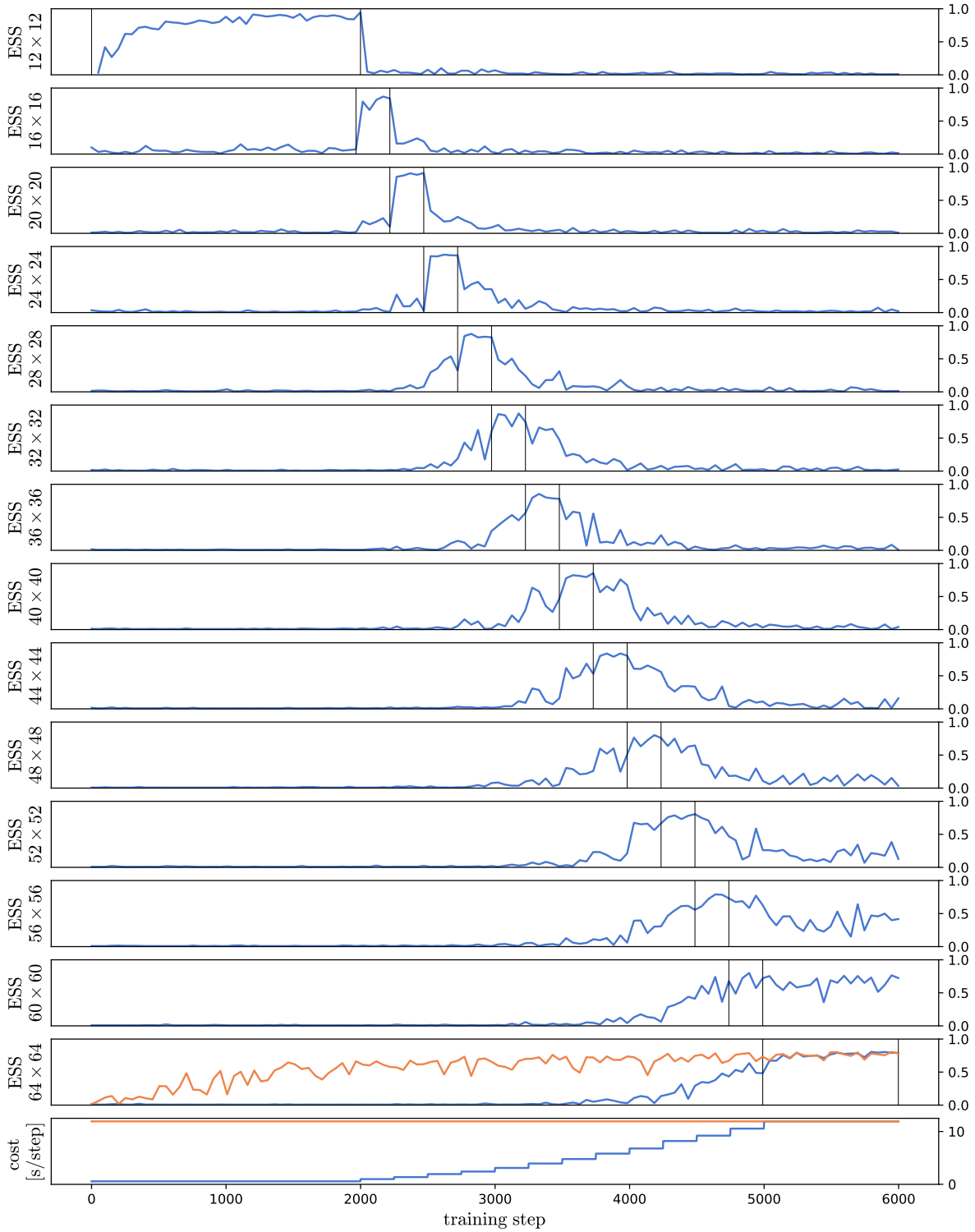


Figure 9: Experiment 4.3. ESS values computed during training from 128 samples on all the lattices the sees during training. The two thin vertical lines denote the interval during which the model is trained on the given lattice size. The orange curve corresponds to the baseline model only trained on the 64×64 lattice.

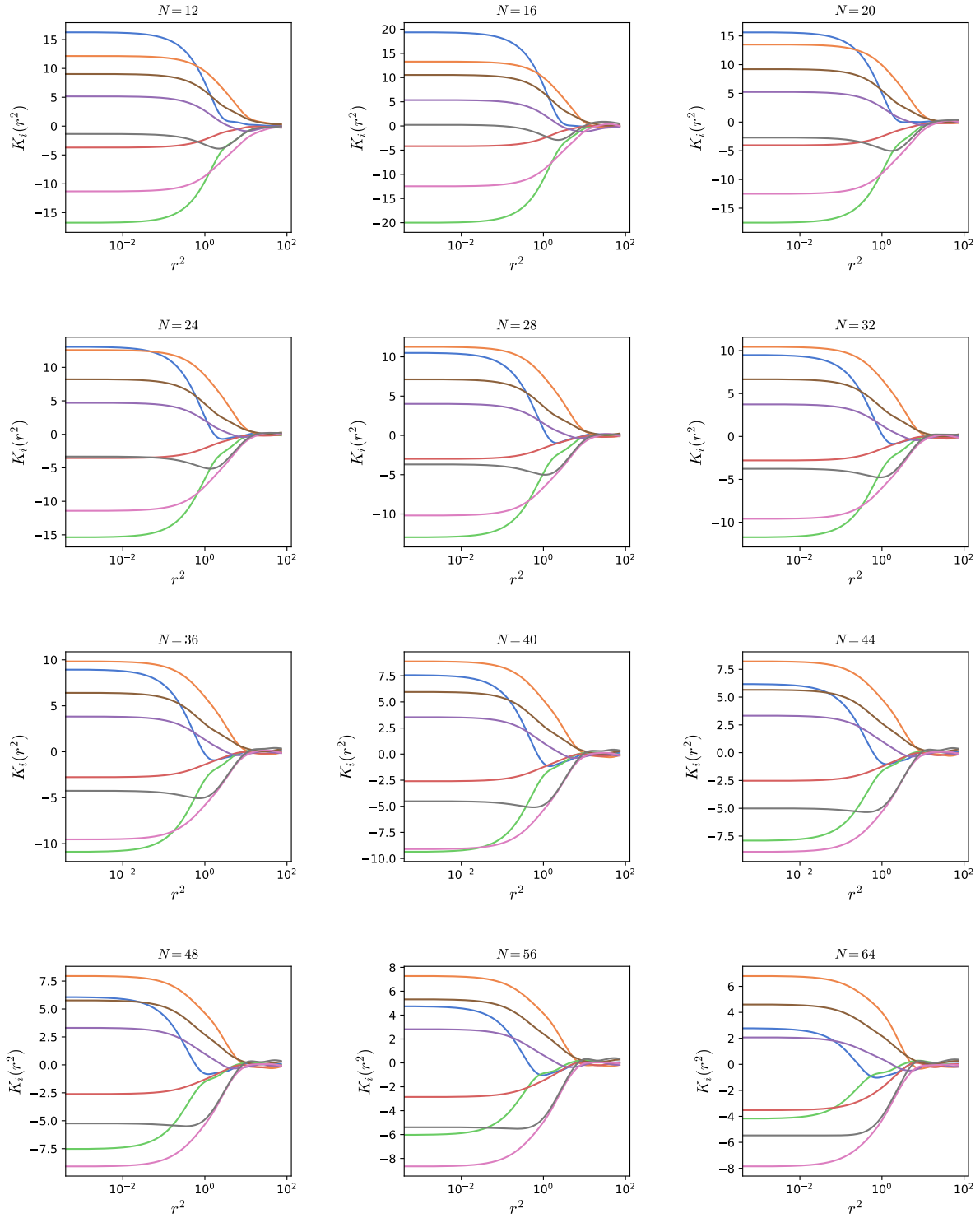


Figure 10: Experiment 4.3. Kernels (Section §3) learnt by the model on various lattice sizes.